


Remarkable disparity in mechanical response among the extracellular domains of type I and II cadherins

Ruchuan Liu , Fei Wu & Jean Paul Thiery


To cite this article: Ruchuan Liu , Fei Wu & Jean Paul Thiery (2013) Remarkable disparity in mechanical response among the extracellular domains of type I and II cadherins, Journal of Biomolecular Structure and Dynamics, 31:10, 1137-1149, DOI: [10.1080/07391102.2012.726530](https://doi.org/10.1080/07391102.2012.726530)

To link to this article: <http://dx.doi.org/10.1080/07391102.2012.726530>

 View supplementary material [↗](#)

 Published online: 04 Oct 2012.

 Submit your article to this journal [↗](#)

 Article views: 88

 View related articles [↗](#)

Remarkable disparity in mechanical response among the extracellular domains of type I and II cadherins

Ruchuan Liu^{a,b}, Fei Wu^b and Jean Paul Thiery^{a,c}

^aMechanoBiology Institute, National University of Singapore, 117411 Singapore ; ^bDepartment of Physics, National University of Singapore, 117542 Singapore; ^cDepartment of Biochemistry, National University of Singapore, 117597 Singapore

Communicated by Ramaswamy H. Sarma

(Received 11 June 2012; final version received 16 August 2012)

Cadherins, a large family of calcium-dependent adhesion molecules, are critical for intercellular adhesion. While crystallographic structures for several cadherins show clear structural similarities, their relevant adhesive strengths vary and their mechanisms of adhesion between types I and II cadherin subfamilies are still unclear. Here, stretching of cadherins was explored experimentally by atomic force microscopy and computationally by steered molecular dynamics (SMD) simulations, where partial unfolding of the E-cadherin ectodomains was observed. The SMD simulations on strand-swapping cadherin dimers displayed similarity in binding strength, suggesting contributions of other mechanisms to explain the strength differences of cell adhesion *in vivo*. Systematic simulations on the unfolding of the extracellular domains of type I and II cadherins revealed diverse pathways. However, at the earliest stage, a remarkable similarity in unfolding was observed for the various type I cadherins that was distinct from that for type II cadherins. This likely correlates positively with their distinct adhesive properties, suggesting that the initial forced deformation in type I cadherins may be involved in cadherin-mediated adhesion.

An animated Interactive 3D Complement (I3DC) is available in Proteopedia at <http://proteopedia.org/w/Journal:JBSD:25>

Keywords: classical type I cadherins; classical type II cadherins; E-cadherin; cell adhesion; homophilic interaction; calcium bridge; SMD simulation; single-molecule force spectroscopy; AFM force mode; unfolding; intermediate state; conformational dynamics; elasticity

Introduction

Classical cadherins are a family of calcium-dependent homophilic cell adhesion molecules, and exert important functions in tissue morphogenesis, neuronal development, and signal transduction (Gumbiner, 1996; Gumbiner, 2005; Pla et al., 2001; Takeichi, 1995). Cadherins are critical for the maintenance of tissue structure and integrity, and the loss of E-cadherin expression, the prototypical epithelial cadherin, has been associated with tumor progression and metastasis of carcinoma (Cowin, Rowlands, & Hatsell, 2005).

The classical cadherin family consists of several subgroups (Nollet, Kools, & van Roy, 2000) including type I (classical) and type II cadherins. Type I cadherins, including E-, N-, and C-cadherin, can establish robust adhesions between cells. In contrast, type II cadherins, including cadherins 6, 7, 8, and 11, are usually associated with much weaker adhesions and found primarily in mesenchymal tissues. For instance, cells expressing

E- and N-cadherins have been shown to mediate much stronger adhesions than cadherin 7, and the extracellular segments of cadherins have been found to dominate the cell adhesive force (Chu et al., 2006). Multiple force measurements have been performed to study the interactions of cadherins at the molecular level by surface force apparatus (Sivasankar, Gumbiner, & Leckband, 2001; Zhu et al., 2003), biomembrane force probe (Bayas, Leung, Evans, & Leckband, 2006; Perret, Leung, Feracci, & Evans, 2004), and atomic force microscopy (AFM) (Baumgartner et al., 2000; Panorchan et al., 2006b; Panorchan, George, & Wirtz, 2006a; Shi, Maruthamuthu, Li, & Leckband, 2010; Sivasankar, Zhang, Nelson, & Chu, 2009; Zhang, Sivasankar, Nelson, & Chu, 2009). These results fail to establish a unique model for the homophilic interaction that occurs.

Despite the apparent difference in adhesion strength, various structural similarities have been identified amongst the extracellular cadherin (EC) domains of types

*Corresponding author. Email: phylr@nus.edu.sg

I and II cadherins. The extracellular segments share five repeated EC domains, which fold in a similar manner (Boggon et al., 2002; Harrison et al., 2011; Hatta, Nose, Nagafuchi, & Takeichi, 1988; Overduin et al., 1995; Patel et al., 2006; Shapiro et al., 1995). In addition, all of the extracellular segments have the capacity to bind 12 Ca^{2+} ions, bridging with these ions via highly conserved residues. Furthermore, most structures to date exhibit a “*trans*” dimer interface by swapping an N-terminal β -strand with its partner, which involves a tryptophan at position two in type I cadherins and tryptophans at positions two and four in type II cadherins (Patel et al., 2006; Shapiro et al., 1995).

This strand-swapping dimer is critical in cadherin-mediated adhesion. A mutation in any of the responsible tryptophan residues in either type I or type II cadherins abrogates the corresponding cell adhesion (May et al., 2005; Shan, Koch, Murray, Colman, & Shapiro, 1999; Tamura, Shan, Hendrickson, Colman, & Shapiro, 1998). These similarities in structure but discrepancies in function indicate that neither the 3D structure nor the homophilic adhesive interface between cadherins can predict the adhesive strength of homophilic interactions between cadherins (Thiery, Engl, Viasnoff, & Dufour, in press).

Cadherin-mediated adhesion is believed to be initiated by the *trans* strand-swapped dimers and later strengthened by *cis*-interactions of the dimers in the formation of lateral clusters (Harrison et al., 2011; Wu, Vendome, Shapiro, Ben-Shaul, & Honig, 2011). However, this model also does not fully explain the significantly different strength in cell adhesion mediated by these two subfamilies of cadherins. Similarly, data from force measurements experiments have yet to elucidate the mechanisms driving cadherin strength of binding.

One essential factor that is absent in all experiments for crystallographic structures is the adhesion forces that cadherins bear *in vivo*. At cell adhesion junctions, conformational changes in cadherins are brought about by adhesion forces. However, how cadherins deform under forces is not clear and cannot presently be ascertained from crystallographic data. Following deformation, it is likely that new surfaces are exposed on cadherins that may be suitable for homophilic interactions between cadherins. This hypothesis is similar to the case that was recently described for the activation of vinculin binding by mechanical stretching of talin rods (del Rio et al., 2009). Therefore, it is fundamental to first determine the elastic properties of cadherins in order to provide a critical step forward in gaining an understanding of the mechanisms of cadherin-mediated adhesion. As yet, only a few studies have attempted unfolding of C-cadherins by AFM and by steered molecular dynamics (SMD) (Oroz et al., 2011; Sotomayor, Corey, & Schulten, 2005; Sotomayor & Schulten, 2008); cadherin 23 has been examined (Sotomayor, Weihofen, Gaudet, & Corey, 2010), as have other

cell adhesion proteins (Gao, Sotomayor, Villa, Lee, & Schulten, 2006). However, a systematic comparison between subfamilies of cadherins may provide insight into the adhesive mechanism of cadherins.

In this report, we carried out SMD simulations and AFM force experiments to investigate the mechanical responses of the cadherin EC domains. The AFM forced unfolding of the full extracellular segment of E-cadherins showed partial unfolding of the EC domains. The unfolding forces were comparable to the unbinding forces of E-cadherin interactions that have been reported previously. The SMD simulations for type I cadherins showed that the unfolding of their first two EC (EC12) domains always began with the unfolding of the two N-terminal β -strands. In contrast, SMD simulations for type II cadherins showed quite different initiations in their unfolding. Given that partial unfolding of E-cadherin EC domains occurred simultaneously with the establishment of their interactions, the difference between types I and II cadherins in the initial unfolding pathway is likely positively correlated with the adhesive strength they mediate. Based on the results, we discuss the possible important intermediate states of cadherin EC domains, their regulation by Ca^{2+} ions, and their possible roles in cadherin-mediated interactions.

Results

The following sections of the SMD simulation results are based on the simulations summarized in Table 1 and the details of the simulations are outlined in the Experimental procedures section.

Forced unbinding of cadherin dimers

In available crystallographic structures, both types I and II cadherins showed a similar tendency to form symmetric *trans* dimers by exchanging their N-terminal β -strands, e.g. a dimer of EC1-2 domains of E-cadherin (Figure 1, inset). An obvious difference between types I and II cadherins has also previously been identified: there are two conserved tryptophans (TRP2 and TRP4) in the swapping β -strand for type II cadherins, while only one (TRP2) for type I cadherins, which results in a larger buried accessible surface area in type II cadherins (Patel et al., 2006). To compare the strength of the strand-swapping dimers, SMD simulations were performed by pulling dimers of E-cadherin (ECAD-D), cadherin 8 (CAD8-D), and 11 (CAD11-D) from their two termini. In these simulations, the dimer structures of EC1–2 domains from the crystallographic data were used (see Simulation procedures for details).

The SMD simulations were repeated several times for each dimer. The trajectories of force vs. extension are shown in Figure 1(a), where extension is the change in end-to-end distance of the protein. In each trajectory, the

Table 1. Summary of SMD simulations on pulling proteins in constant-velocity mode.

Label	Structure	Type	Size (\AA^3)	Atoms \times 1000	Ensemble	Spring constant (pN/ \AA)	Pulling speed ($\text{\AA}/\text{ps}$)	Time (ns)
ECAD	2QVF	PCV	$691 \times 73 \times 65$	315	NV	69.5	0.1	6
ECAD-NOCA	2QVF	PCV	$689 \times 64 \times 74$	314	NV	69.5	0.1	6
ECAD-D	2QVF	PCV	$205 \times 55 \times 76$	82	NV	69.5	0.1	0.5 ^b
ECAD-D	2QVF	PCV	$236 \times 74 \times 58$	96	NV	69.5	0.05	0.8 ^b
ECAD-D	2QVF	PCV	$192 \times 85 \times 108$	166	NV	3.495–13.9	0.0025–0.025	5–50 ^b
CAD8	2A62-S ^a	PCV	$799 \times 71 \times 81$	445	NV	69.5	0.1	6
CAD8-D	2A62-S ^a	PCV	$238 \times 64 \times 55$	81	NV	69.5	0.1	0.9
CAD11	2A4E	PCV	$787 \times 64 \times 77$	375	NV	69.5	0.1	6
CAD11-D	2A4E	PCV	$212 \times 71 \times 52$	75	NV	69.5	0.1	0.9
CCAD	1L3 W ^{-a}	PCV	$700 \times 80 \times 61$	326	NV	69.5	0.1	6
NCAD	2QVI	PCV	$691 \times 82 \times 80$	440	NV	69.5	0.1	6

Notes: Available crystallographic structures were chosen for SMD simulation. The EC1–2 domains of type I: E-cadherin with (ECAD) or without Ca^{2+} ions (ECAD-NOCA), N-cadherin (NCAD), and C-cadherin (CCAD). EC1–2 domains of type II: cadherin 8 (CAD8) and cadherin 11 (CAD11) as well as their dimers (with additional “-D” indicated). All structures were equilibrated from solvated crystallographic structures using a constant NpT ensemble for about 0.6 ns before simulations. The final constant-velocity simulations were performed using the particle mesh Ewald method for the long-range electrostatic interactions, while the constant number and volume (NV) ensemble were used. Ensembles are denoted according to the thermodynamic quantity held constant (N , number of particles; p , pressure; T , temperature; and V , volume).

^aFor C-cadherin and cadherin 8, although crystallographic data show more domains, only EC1–2 domains were used for easier comparison with other cadherins.

^bDifferent spring constant and pulling speed have been used to repeatedly stretch the ECAD-D dimers by varying the loading rate. The size of the pulling box is varied to avoid the protein moving out of the water box during simulations when springs of smaller spring constant were used.

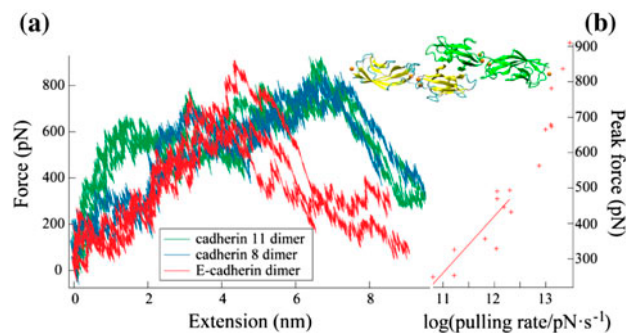


Figure 1. Forced unbinding of cadherin dimers of EC1–2 domains. (a) Trajectories of force vs. extension for SMD simulations on pulling dimers of E-cadherin (red, three trajectories), cadherin 8 (blue, two trajectories), and cadherin 11 (green, two trajectories) at a constant velocity of 0.1 $\text{\AA}/\text{ps}$ using a spring with $k=69.479 \text{ pN}\cdot\text{\AA}$. Here, forces increased first due to the elasticity of proteins and then decreased from the maximum as the dimer interactions broke. Both type II cadherin simulations showed a slightly higher average peak force and a much larger extension at the force peak than E-cadherin. (b) The peak forces from various SMD simulations of pulling the E-cadherin dimers vs. the logarithm of the effective loading rates (pN/s). The unfolding force decreased as the loading rate decreased. The lowest unfolding force in simulations was around 250 pN. The inset structure shows the E-cadherin dimer used in the above SMD simulations with one monomer colored by its secondary structure and the other one mono-colored in new cartoon presentation. Both dimers of cadherin 8 and 11 showed similar overall structures, except that larger binding interfaces were expected (Patel et al., 2006).

force increased until unbinding of the dimer occurred and then the force decreased again. The trajectories from two type II cadherins, CAD8-D (blue curves) and

CAD11-D (green curves), were similar to each other. In these trajectories, unbinding forces (peak forces) reached $\sim 800 \text{ pN}$ at an extension of $\sim 7 \text{ nm}$. Unlike the two type II cadherins, for ECAD-D, variations were observed between three trials and the force peak located at an extension of $\sim 4 \text{ nm}$. However, the average peak force for ECAD-D was close to those forces measured for CAD8-D and CAD11-D. Similar dissociation forces were also reported for C-cadherin dimers (Bayas, Schulten, & Leckband, 2004).

The common and efficient condition for SMD simulation adopted here was dramatically different from other experimental conditions in single-molecule force measurements by AFM, optical tweezers, and magnetic tweezers. In particular, the loading rate, which is the rate of changing force (pN/s), used in the above simulations was $\sim 10^{13} \text{ pN/s}$. This was several orders of magnitude faster than that used in AFM experiments, which is typically in the range of $10^3\text{--}10^4 \text{ pN/s}$. Due to limitations in computational power, it is still not practical for computational simulations to be done at a loading rate similar to these experimental conditions. We were thus able to lower the loading rate to $\sim 6.4 \times 10^{10} \text{ pN/s}$, and the dissociation force observed was around 250 pN. Figure 1(b) summarizes the peak forces vs. the logarithm of effective loading rates obtained from the simulation trajectories. There is a clear trend for a decrease in the dissociation force with a lower loading rate.

Unfolding of E-cadherin and the role of Ca^{2+} ions

To ascertain the mechanical strength and response of E-cadherin EC domains, single-molecule AFM pulling

experiments were performed. Similar force spectroscopy experiments have been previously carried out successfully with monomers of other proteins (Garcia-Manyes, Brujic, Badilla, & Fernandez, 2007). We chose to use monomers of the full extracellular segment of E-cadherin for the experiment, as constructs of repeated modules of each EC domain would significantly alter the binding sites for Ca^{2+} ions, leading to changes in its mechanical properties. The extracellular segments in stretching included all the five similar but not identical EC domains. Control experiments, including pulling by magnetic tweezers, were carried out to ensure that the majority of events observed in the experiments were from the E-cadherin domains (Wu et al., 2012).

In the force vs. extension trajectories (Figure 2(a), inset), typical saw-tooth patterns were observed. The contour length changes (ΔL) of each unfolding event were calculated using the worm-like chain (WLC) model (Rief, Gautel, Oesterhelt, Fernandez, & Gaub, 1997). Figure 2 shows the histograms of unfolding forces and ΔL . The unfolding forces showed a broad distribution, with the majority of the forces below 160 pN. The histogram of ΔL was fitted by multi-Gaussian distributions that peaked around 12, 20, 31, and 39 nm.

The adhesion function of cadherins is regulated by Ca^{2+} ions (van Roy & Berx, 2008), which function to stabilize their extracellular segments. Previous crystallographic data have shown that Ca^{2+} ions form bridges with highly conserved residues in cadherins (Boggon et al., 2002; Harrison et al., 2011; Patel et al., 2006). The SMD simulations were also used to unfold E-cadherin EC1–2 domains (ECAD) in the presence of four Ca^{2+} ions (Figure 3). A force vs. extension trajectory (black curve) from a typical simulation ($k=64.9 \text{ pN/\AA}$ and $v=0.1 \text{ \AA/ps}$) featured five force peaks of ~ 1780 , ~ 1450 , ~ 1180 , ~ 1290 , and $\sim 1720 \text{ pN}$ (Figure 3(a), black curve). The majority of unfolding events resulted in extension changes between 8 and 22 nm, with an average of 12 nm. This was in agreement with the first peak by multi-Gaussian fitting of the histogram of ΔL from AFM experiments. In AFM experiments, multiple unfolding steps could take place simultaneously, resulting in a larger ΔL (31 and 39 nm).

Snapshots from this particular trial of the unfolding of ECAD are shown in Figure 3(b)–(k). The images show a few residues interacting with Ca^{2+} ions (highlighted in licorice representation). The first EC (EC1) domain unfolded first, followed by the second EC (EC2) domain, with EC domain unfolding occurring in a step-wise manner. Each force peak in the trajectory is associated with the detachment of a couple of β -strands or more from the structure. For example, this unfolding began with the detachment of the first two β -strands near the N-terminus, with the rupture of both hydrogen bonds

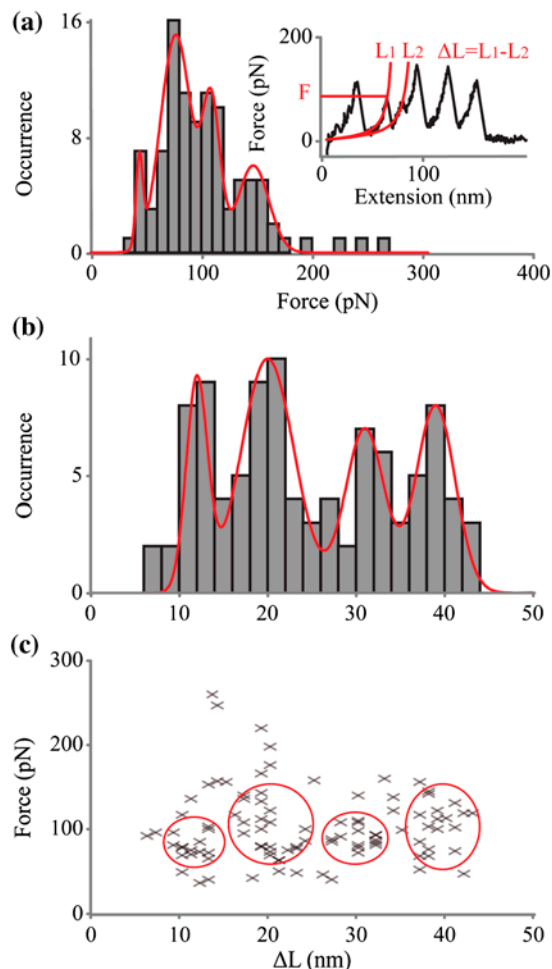


Figure 2. AFM unfolding of full ectodomains of E-cadherins. (a) The histogram of unfolding forces. The histogram was fitted by four Gaussian distributions (red curves), which peaked at 44, 77, 109, and 147 pN, respectively. The inset shows a typical force-extension curve obtained. The force peaks were fitted by the WLC model with different contour lengths, e.g. L_1 and L_2 (red). The contour length increase between two sequential peaks was caused by the unfolding event corresponding to the prior one. The unfolding force, F (red), and the contour length change, ΔL , were recorded. (b) The histogram of unfolding contour length change, ΔL . The histogram was fitted by Gaussian distributions (red curve), which peaked at 12, 20, 31, and 39 nm, respectively. All measurements were obtained in a HEPES buffer with pH 7.4 and 1 mM Ca^{2+} . The pulling velocity is 600 nm/s. (c) The scatter plot of unfolding force vs. contour length shows roughly four groups corresponding to the four contour length peaks in the histogram in (b). The total events number is 98.

among β -strands and Ca^{2+} bridges. Figure 3(c) and (d) shows the disruption in the interaction between Ca^{2+} ions and Glu11, corresponding to the first force peak in Figure 3(a). Similar disruptions of Ca^{2+} -associated bridges occurred sequentially as unfolding progressed (e.g. from Figure 3(g)–(k)).

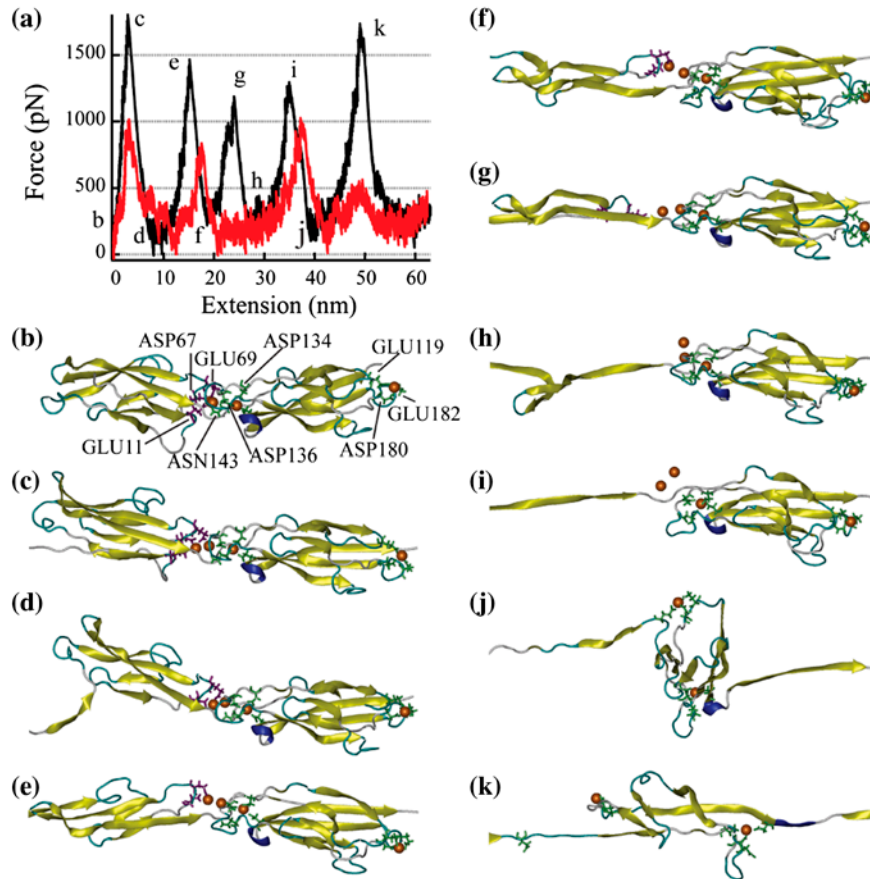


Figure 3. Unfolding of E-cadherin EC12 domains. (a) Force vs. extension trajectories from constant-velocity stretching, with crystallographic Ca²⁺ ions (black) or without (red). (b)–(k) Snapshots of the unfolding pathway for this particular trial of ECAD, including crystallographic ions (orange balls), with only the region of the remaining folded structures captured. The time spot of each snapshot is labeled in (a). The views show the EC1–2 domains of E-cadherin in new cartoon representation using the secondary structure of the unstretched protein; the extended part, if at two sides, is chopped off in the snapshots to highlight the structures remaining folded. Specific residues that interacted with the Ca²⁺ ions are labeled and shown in licorice presentation: three residues from the EC1 domain (purple: GLU11, ASP67, and GLU69) and seven residues from the EC2 domain (lime: GLU119, ASP134, ASP136, ASN143, ASP180, GLU182, and ASP195), while there were still several residues (not labeled) from the linker regions between domains that also interacted with the Ca²⁺ ions. Each force peak in (a) involved a couple of β-strands detached from other strands. Also, the breaking of bridges with the Ca²⁺ ions can be found from (c) to (d); from (g) to (h); from (i) to (j); and from (k) to fully extended.

A trajectory (red curve) was also plotted for the SMD simulation of E-cadherin EC1–2 domains without Ca²⁺ ions (ECAD-NOCA) (Figure 3(a)). The results showed significantly reduced forces with only four peaks of ~990, ~830, ~1000, and ~500 pN. Although the force vs. extension trajectories of ECAD and ECAD-NOCA appear similar, the removal of Ca²⁺ ions dramatically altered the unfolding pathway (see movies of ECAD and ECAD-NOCA unfolding, Supplemental Information) with differences in the order of the partial unfolding steps. For instances, the unfolding steps of EC1 took place before those of EC2 for ECAD, while the opposite was observed for ECAD-NOCA; this indicates that Ca²⁺ bridges stabilize the EC2 domain more than the EC1 domain of E-cadherin.

Unfolding of types I and II cadherins

The SMD simulations at a similar condition were also repeated for EC1–2 domains of several cadherins for which the structure was available: ECAD, N-cadherin (NCAD), C-cadherin (CCAD), cadherin 8 (CAD8), and cadherin 11 (CAD11). Figure 4 shows their force-extension trajectories from the constant-velocity pulling simulations; trajectories with colors represent different trials of simulations. Significant differences in unfolding forces were found between cadherins from these two subfamilies. Both type II cadherins, CAD11 (Figure 4(d)) and CAD8 (Figure 4(e)), showed a much stronger unfolding force at ~3000 pN or more, than type I cadherins (Figure 4(a)–(c)), which were ~2500 pN or less.

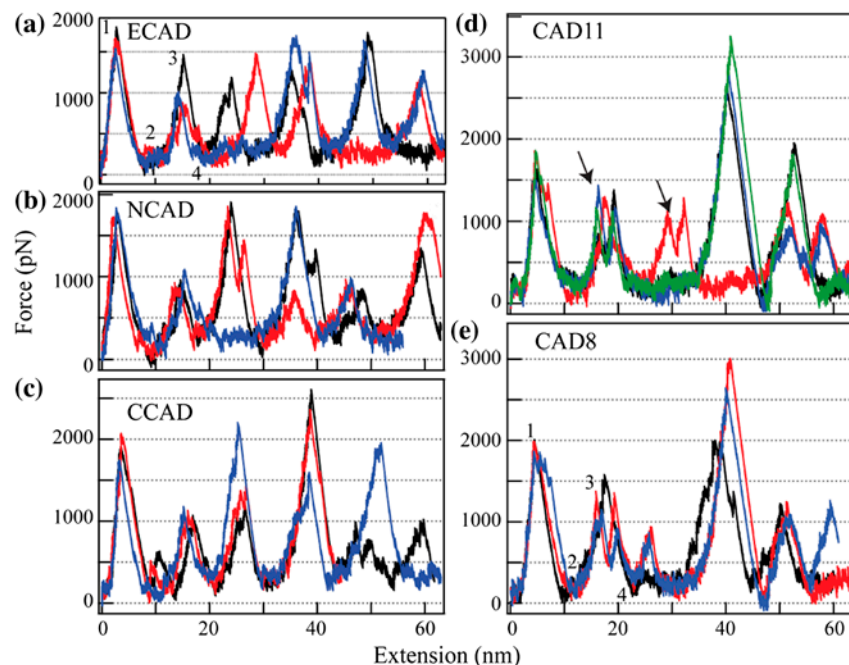


Figure 4. Unfolding trajectories of EC1–2 domains of type I and II cadherins by stretching at a constant velocity. (a) E-cadherin with four Ca^{2+} ions. Different unfolding patterns after the first unfolding peak were observed. (b) The unfolding pattern of N-cadherin, with three Ca^{2+} ions, similar to E-cadherin varied among the trajectories. (c) C-cadherin, with six Ca^{2+} ions showed three similar trajectories; (d) Cadherin 11, with three Ca^{2+} ions, showed four similar trajectories, with the exception of the one in red; (e) Cadherin 8, with six Ca^{2+} ions, showed three similar trajectories, with the exception of the one in black. Type II cadherins showed much higher maximal peak forces in unfolding than the type I cadherins. Most trajectories from type II cadherins showed similar patterns. Colors of curves are used to distinguish different trials of SMD simulation on the same protein. In (a) and (e), numbers 1–4 label the time spots for snapshots in Figure 5.

On the other hand, these trajectories shared a few common features: (1) each trace showed five to six force peaks; (2) the first two peaks presented with similarities between the traces; and (3) most of the first peaks were similar in shape and peak force. The slight variations in the positions of the first peaks were likely due to different initial alignments of the EC domains along the stretching direction. In addition, trajectories from the same subfamily shared more similar features. Traces in Figure 4(d) (CAD11, except the red one) and Figure 4(e) (CAD8, except the black one) were similar in appearance. Similar patterns were also observed at different extensions (for example, two peaks in all curves in Figure 4(d) (arrow)).

Unfolding pathways: differences and similarities

Interesting observations were made for the detailed unfolding pathways (as shown in movies of SMD simulations; see Supplemental Information). A key difference between type I and II cadherins was observed at the beginning of unfolding. The EC1–2 domains of ECAD, NCAD, and CCAD demonstrated a unique start in the process of unfolding, involving the detachment of the

two N-terminal β -strands. The first force peaks in the unfolding of types I cadherins (Figure 4(a)–(c)) were from the unfolding of the EC1 domain. However, for type II cadherins, unfolding most likely started from the EC2 domain. The first force peaks in unfolding of CAD8 and CAD11 (Figure 4(d) and (e)) were mostly from the unfolding of the EC2 domain and the highest force peaks resulted from the unfolding of the EC1 domains. Interestingly, the unfolding pathways of ECAD-NOCA (without Ca^{2+}) were most reminiscent of the unfolding for type II cadherins.

Snapshots for ECAD and CAD8 were taken over three trials to represent the early stages of the unfolding (Figure 5, rows). Four time spots (Figure 5, columns 1–4) were chosen similar to those in Figure 3(c)–(f), and refer to the time spots labeled in the trajectories (Figure 4 (a) and (e)). All snapshots were chopped at the two sides to only include the folded part of the constructs. In Figure 5, all trajectories of ECAD began unfolding with the detachment of the first two β -strands. In contrast, unfolding of CAD8 commenced at the inter-junction between the EC1–2 domains; in two trials, unfolding occurred from the EC2 side and in one trial, from the EC1 side of the inter-junction.

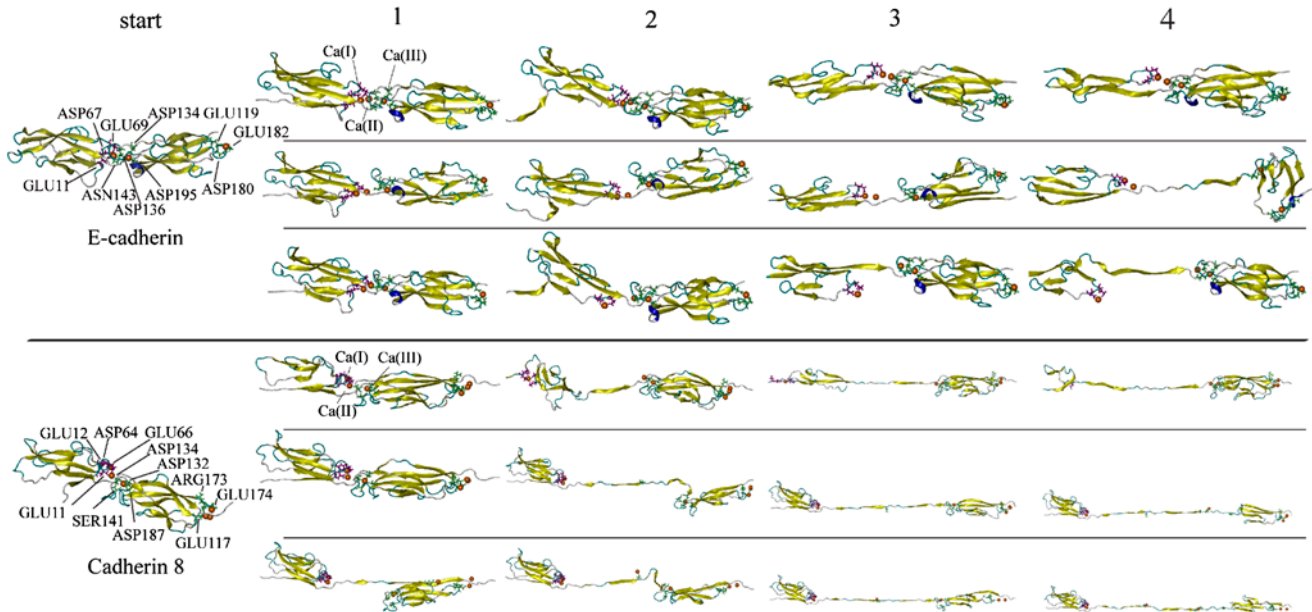


Figure 5. Comparison of unfolding pathways among trials of stretching E-cadherin and cadherin 8 at a constant velocity. Each row represents snapshots from one trial recorded in SMD simulations, while columns 1–4 represent time spots indicated on the trajectories in Figure 4. The top three trials are from simulations of ECAD, while the very top one is the same as the snapshots shown in Figure 3(c)–(f), and the bottom three are from those of CAD8. All views show the EC1–2 domains of cadherins in new cartoon representation using the secondary structure of the unstretched proteins, which are the two start structures. The extended part of the EC1–2 domains, if at two sides, was chopped off to highlight the structure remaining folded. Similar to Figure 3, specific residues that interacted with the Ca^{2+} ions are shown in licorice presentation: residues from the EC1 domain are labeled in purple and from those from EC2 domain in lime.

Discussion

Homophilic interactions between cadherins

Crystallographic data show that the buried accessible area for head-to-head dimers of a few type II cadherins is larger than that for type I cadherins (Patel et al., 2006). This indicates that the strand-swapping dimer of type II cadherins may be mechanically stronger or, at least, not weaker. Our simulation results (Figure 1(a)) show comparable forces for detaching strand-swapping dimers of ECAD, CAD8, and CAD11. In addition, similar dissociation forces have been observed in SMD simulations on C-cadherin dimers (Bayas et al., 2004). Thus, the binding strength of strand-swapping dimers of types I and II cadherins are likely comparable to each other. Therefore, from a structural point of view, types I and II cadherins are quite alike, with similar sequences and folded structures; highly conserved residues for Ca^{2+} bridges (Patel et al., 2006); similar head-to-head dimers by strand swapping; and now even comparable detachment forces. However, cell adhesion mediated by type I cadherins is believed to be stronger than that mediated by type II cadherins. For example, cell adhesion mediated by E-cadherin is much stronger than that mediated by cadherin 7 (Chu et al., 2006). Therefore, the head-to-head dimers, as pictured by the crystallographic data, are

unlikely to be the only or dominant homophilic interactions between cadherins.

In this study, we attempted SMD simulations on ECAD-D using different pulling rates. By lowering the loading rate from 3×10^{13} to 6.4×10^{10} pN/s, the dissociation force decreased from ~ 900 to ~ 250 pN. In single cell/single molecule AFM experiments, at a loading rate around 10^4 pN/s, homophilic interactions between E-cadherins have been shown to break at a peak force above 180 pN (Panorchan et al., 2006b). Although there is still a huge gap in loading rates between SMD simulations and AFM experiments, the observed peak forces have already become quite close. Likely, further reductions of the loading rate in SMD simulations may result in a dissociation force of ECAD-D lower than 180 pN. This implies that the cadherin–cadherin interaction measured in AFM experiments is possibly different from the strand-swapping dimer. Thus, this means that mechanisms in addition to the head-to-head dimers likely contribute to the interactions. This is in agreement with the model of strengthening for adhesive interactions by lateral clusters (Wu et al., 2011; Zhang et al., 2009). However, the lateral cluster model may not be the only strengthening mechanism. Surmounting evidence from molecular force experiments of cadherin–cadherin interactions also suggest much more complicated structures

rather than head-to-head dimers (Baumgartner et al., 2000; Evans & Calderwood, 2007; Panorchan et al., 2006b; Perret et al., 2004; Shi et al., 2010; Sivasankar, Briehar, Lavrik, Gumbiner, & Leckband, 1999). For example, all five EC domains have been suggested to contribute to the homophilic interactions of E-cadherins (Perret et al., 2004) and C-cadherins (Shi et al., 2010).

Partial unfolding of E-cadherin ectodomains

The AFM unfolding results of the full extracellular segment of E-cadherin, including all five EC domains, showed that the majority of unfolding forces ranged from 50 to 160 pN. The effective loading rates used were in the range of 10^3 – 10^4 pN/s. At similar loading rates, AFM pulling experiments have also been used to break individual homophilic interactions between E-cadherin molecules (Panorchan et al., 2006b), and the detaching forces measured are comparable with the unfolding force observed for E-cadherin EC domains. Magnetic tweezers experiments have also been carried out, whereby the extracellular segment of E-cadherins is stretched at low forces of ~ 5 pN (Wu et al., 2012). Both unfolding and refolding have shown rates of ~ 0.03 s $^{-1}$; the average time for unfolding and refolding is faster than the maturation time of cell adhesion, which is measured to be ~ 30 min (Chu et al., 2004, 2006). Thus, very likely, unfolding of the E-cadherin EC domains may accompany cadherin–cadherin interactions in cell adhesion. While no unfolding events were reported previously when the detaching forces were measured for E-cadherin (Panorchan et al., 2006), unfolding events might have been neglected during the data analysis. This may be because it was hard to distinguish serial multiple unbinding events and unfolding of the proteins in AFM measurements; trajectories with multiple force peaks were usually excluded when selecting single unbinding events.

Each EC domain consists of ~ 110 amino acids. The physical size of a native EC domain is ~ 3 – 5 nm. Therefore, the contour length change following a one-step unfolding for each EC domain should be close to 38 nm; this corresponds to the last Gaussian peak in Figure 2(b). The majority of the unfolding events (Figure 2(b)) showed smaller ΔL values, indicating that the EC domains are only partially unfolded in those steps. Consequently, on the one hand, the partial unfolding of the E-cadherin EC domains may lead to the dissociation of the interactions. However, on the other hand, partial unfolding of any EC domain also results in intermediate states with some structures maintained; this exposes new hydrophobic surfaces. Some of these newly exposed surfaces may be suitable for new binding interactions which is similar to the activation of vinculin binding by stretching talin rods (del Rio et al., 2009).

Unfolding pathways of cadherins

The SMD simulations of stretching of ECAD, NCAD, CCAD, CAD8, and CAD11 were performed to investigate details in unfolding pathways, such as the existence of intermediate states. Very complicated unfolding pathways were found (Movies, Supplemental Information). However, one similarity was observed among the unfolding of type I cadherins: the unfolding always began with the first two β -strands at the N-terminus. In contrast, type II cadherins did not follow this pattern; rather, their EC2 domains usually unfolded first. The order of this unfolding indicates the relative mechanical stability of the EC domains. Simulations on individual EC1 and EC2 domains of C-cadherins have shown smaller unfolding forces for the EC1 domain (Sotomayor et al., 2005; Sotomayor & Schulten, 2008). In type II cadherins, the unfolding forces for EC1 domains were much higher than those for EC2 domains (Figure 4(d) and (e)) and those for EC1 domains of type I cadherins (Figure 4(a)–(c)). This also sounds interesting, so we are performing further SMD simulations to compare individual EC domains in mechanical stability. In addition, most unfolding trajectories of these cadherins showed that the weakest point in the EC1 domains was the two N-terminal β -strands. Somehow, this is strengthened in type II cadherins. One of the strengthening factors could be the additional Ca^{2+} bridge at the interdomain region of type II cadherins. This will be discussed later.

Unlike those structural similarities, the differences during the initiation of the unfolding do not conflict with the strength of cell–cell adhesion. Rather, such differences seem to be positively correlated with the distinctive adhesive functions between these subfamilies of cadherins, because the partial unfolding of the EC domains likely takes place during the maturation of cell adhesion. Thus, we suggest that the detachment of the N-terminal two β -strands or the resultant intermediate states may be very important in terms of the association with the adhesive properties of cadherins.

The role of Ca^{2+} ions

The presence of Ca^{2+} ions is necessary for the adhesive function of cadherins. In Figure 3(a), a comparison between E-cadherin with and without Ca^{2+} ions directly proved that Ca^{2+} can greatly increase the mechanical stability of cadherins; this is consistent with the previous simulations on C-cadherins (Sotomayor et al., 2005; Sotomayor & Schulten, 2008). Also, the removal of Ca^{2+} significantly reduced the peak force of the first unfolding event from ~ 1800 to ~ 1000 pN (Figure 3(a)), making it closer to the dissociation force of the strand-swapping dimer (Figure 1(a)) at a similar stretching condition in simulations.

It seems that the three Ca^{2+} ions at the junction between the EC1 and the EC2 domains play a different role. From the snapshots of trajectories of pulling ECAD and CAD8, it appears that during the unfolding processes Ca(III) maintains close contact with the EC2 domain, while Ca(I) with the EC1 domain. Further, the removal of Ca^{2+} ions in ECAD resulted in an unfolding pattern for ECAD-NOCA that was reminiscent of that of type II cadherins. This indicates that in ECAD, Ca(III) may stabilize the EC2 domain and changes the order of unfolding for EC1 and EC2 domains. In the case of type II cadherins, the stabilization of the EC1 domains by Ca(I) and Ca(II) may be more prominent.

Therefore, the role of Ca^{2+} ions goes beyond stabilization. The availability and the fluctuation of Ca^{2+} bridges as well as the variation in their strength likely introduces more flexibility in unfolding, as shown in Figure 5, because most of the unfolding steps are associated with the breaking of Ca^{2+} bridges. In Figure 5, the breaking order of the Ca^{2+} bridges varied in different trials, with the exception that the bridges between Ca(I), Ca(II), and Glu11 always broke first upon detachment of the two N-terminal strands during ECAD unfolding. In type II cadherins, an additional bridge was observed between Ca(I) and Glu12 that likely strengthens the connection of the two N-terminal β -strands to the joint domain region. As such, the bridges become more difficult to break simultaneously during unfolding of type II cadherin. Furthermore, a Glu12 mutation in type II cadherins may weaken the connection of the two N-terminal strands and change the unfolding pathway to become more like type I cadherins.

The affinity of the Ca^{2+} ion binding sites at the interjunction of the E-cadherin EC1–2 domains has been measured experimentally (Koch, Pokutta, Lustig, & Engel, 1997). Among them, the two sites show similar affinity with a k_{ds} of $\sim 330 \mu\text{M}$ and the other one with a k_{ds} of $\sim 2 \text{mM}$, respectively. Cailliez et al. proposed Ca(I) as having the lowest affinity (Cailliez & Lavery, 2005). These differences in Ca^{2+} affinity are in agreement with the results from our SMD simulations. As compared with the other two Ca^{2+} ions, Ca(I) is associated with weaker bridges, which are broken at the early stage of unfolding of ECAD. In experiments *in vivo* and *in vitro*, buffers with 1 mM Ca^{2+} ions are usually used for E-cadherins, so the binding sites for Ca^{2+} ions may be partially occupied, e.g. the site for Ca(I). This can result in more easily detached N-terminal β -strands. Furthermore, thermal fluctuations in Ca^{2+} bridges and binding/unbinding dynamics of Ca^{2+} ions may temporarily introduce weak points in the structure and lead to a more complicated mechanical response of cadherins.

Cadherin–cadherin interaction *in vivo*

The β -strand swapping dimers of cadherins are essential in the development of cell adhesion, especially in the initial stage. It has been suggested that these *trans* dimers can further interact in *cis* to form lateral clusters in cadherin-mediated adhesion (Wu et al., 2011). However, to explain the distinct strength between types I and II cadherins, additional mechanisms are needed. Studies have shown that vinculin recruitment is activated due to the exposure of new binding sites after the unfolding of talin rods (del Rio et al., 2009), and we speculate that a similar mechanism may exist in strengthening cadherin-mediated adhesion.

Cadherin EC domains should experience forces at various directions during cell adhesions *in vivo*. For example, if lateral clusters of cadherins are formed by their *cis*-interactions (Harrison et al., 2011; Wu et al., 2011), the *cis*-interactions will cause deviations in the force direction even though the opposite cells may stretch the strand-swapping dimers of cadherins from the two ends as in our simulations. In our study, the AFM results indicated that partial unfolding of E-cadherin EC domains likely accompanies their homophilic interactions and the SMD simulations revealed that the connection of the two N-terminal β -strands to the EC1 domain is the weakest point. Consequently, the forced partial unfolded state with the two N-terminal β -strands detached may be among one of the intermediate states that strengthen cadherin-mediated adhesion. In type II cadherins, the conserved Glu12 introduces more Ca^{2+} bridges between cadherins and Ca(I), therefore making similar intermediate states less likely. Thus, such a hypothesis in addition to the present understanding of cadherin-mediated adhesion can explain the difference in adhesive strength associated with cadherin subfamilies.

In summary, our results from AFM force experiments on E-cadherins show partial unfolding of EC domains and the unfolding forces are comparable to the dissociation forces of E-cadherin interaction measured by AFM (Panorchan et al., 2006b). This suggests that partial unfolding of E-cadherin EC domains likely occurs during the dynamics of E-cadherin-mediated adhesion. The SMD simulations also confirm the partial unfolding and show a clear disparity in unfolding pathways between types I and II subfamilies of cadherins, which seems to correlate with the differences in their adhesive properties. Particularly, beyond rigidifying the EC domains of cadherins, Ca^{2+} ions regulate the availability of intermediate states in partial unfolding. We believe that intermediate states from partial unfolding may also participate in cell adhesions, providing new binding interfaces to strengthen cadherin-mediated adhesion.

Simulation procedures

Simulated systems

All structures used in simulations were from crystallographic data available in the protein data bank, and only EC1–2 domains of cadherins were included with the resolved Ca^{2+} ions, except as otherwise stated. All dimers in simulations were assembled by two EC1–2 domains of cadherins binding through a strand-swapping mechanism, as suggested by the crystallographic structures.

Monomers and dimers were derived from extracellular domains of E-cadherin (PDB code 2QVF), including residues 1–213. The first structure, referred to as ECAD, encompassed the EC1–2 domains along with four crystallographic Ca^{2+} ions, three of which were located at the first interdomain junction. The second structure was the same, except without Ca^{2+} ions, and thus referred to as ECAD-NOCA. The third structure was the homophilic dimer of E-cadherin EC1–2 domains assembled by swapping a β -strand between the EC1 domains as suggested by the crystal structures of E-cadherin and the other type I cadherins. This structure of E-cadherin EC1–2 was referred to as ECAD-D.

The next two structures were dimers assembled from EC1–2 domains of two type II cadherins, cadherin 8 (PDB code 2A62) and cadherin 11 (PDB code 2A4E) (Patel et al., 2006), and were referred to as CAD8-D and CAD11-D, respectively. Each monomer in CAD8-D included residues 1–213 as well as six Ca^{2+} ions at the first two interdomain junctions. Each monomer in CAD11-D included residues 0–207 as well as three Ca^{2+} ions at the first interdomain junction. Another two structures were monomers of EC1–2 domains from both type II cadherins with Ca^{2+} ions and were referred to as CAD8 and CAD11, respectively.

The last two structures were derived from the extracellular domains of another two type I cadherins, N-cadherin (PDB code 2QVI) and C-cadherin (PDB code 1L3W; Boggon et al., 2002), and were referred to as NCAD and CCAD, respectively. The NCAD included residues 1–215 of N-cadherin, along with three Ca^{2+} ions at the first interdomain junction, and the CCAD included residues 1–217 of C-cadherin, along with six Ca^{2+} ions at the first two inter-domain junctions.

The orientation of all corresponding structures was aligned for stretching along the x-axis. The aligned proteins were then solvated using the visual molecular dynamics (VMD) plugin, solvate (Humphrey, Dalke, & Schulten, 1996). Using the VMD plugin, autoionize, counterions, and 0.1 M NaCl were placed into the systems for neutralization.

Molecular dynamics

The program, NAMD 2.7 and 2.8 (Phillips et al., 2005), was used for SMD simulations of cadherins, together

with the CHARMM27 force field for proteins (Macke-rell, Feig, & Brooks, 2004) and TIP3P model for water molecules (Jorgensen, Chandrasekhar, Madura, Impey, & Klein, 1983) with SHAKE enabled.

van der Waals interactions were cut-off at a distance of 12 Å and the switching function was enabled at 10 Å. All simulations were carried out in periodic boundary conditions with distances between periodic images of the protein always greater than 25 Å. Long-range electrostatic forces were computed with the particle mesh Ewald (PME) method and no cut-off was assumed. Also, in PME, the grid points had a density not less than 1 \AA^{-2} in all cases to ensure the accuracy of the calculation.

A multiple time-stepping algorithm was applied in all simulations: interactions involving covalent bonds and short-range nonbonded interactions were computed for every time step (2 fs) and long-range electrostatic forces were computed at every two time steps. Compared with single time-stepping algorithm, the multiple time-stepping algorithm improved the simulation speed while maintaining accuracy.

Each solvated structure was equilibrated in the constant number, pressure, and temperature (NpT) ensemble for about 0.6 ns, and the resulting state was used in subsequent SMD simulations. Langevin dynamics was enabled for constant temperature ($T=310 \text{ K}$) conditions and 1 ps^{-1} was chosen for the damping coefficient to speed up the conformational changes of the structures by reducing the solvent viscosity. For constant pressure simulations, the hybrid Nosè–Hoover Langevin piston method was used to keep the pressure at 1 atm with a decay period of 200 fs and a damping time constant of 100 fs. All SMD simulations were carried out by stretching at a constant velocity. The spring constant and the pulling speed used were usually $k=69.5 \text{ pN/\AA}$ and $v=0.1 \text{ \AA/ps}$, respectively, unless otherwise stated (e.g. in the study of the dependency on loading rate). For monomers (ECAD, ECAD-NOCA, CCAD, NCAD, CAD8, and CAD11), simulations were done by fixing the N atom of the N-terminal residue and stretching the C_α atom of the C-terminal residue; for dimers (ECAD-D, CAD8-D, and CAD11-D), simulations were done by fixing one of the C_α atoms of C-terminal residues and stretching the other. In all simulations, coordinates of structures were saved every picosecond. Table 1 lists all of the conditions in the SMD simulations.

The program VMD (Humphrey et al., 1996) was used to analyze the simulation trajectories. The extensions were computed as the changes of end-to-end distance. The loading rate in constant-velocity stretching was measured by the slope of a linear fitting before the maximal force in the force vs. time trajectories.

Experimental procedures

Protein expression and purification

A polymerase chain reaction (PCR) product encoding EC1–5 of E-cadherin with additional three cysteine residues at the N-terminus was cloned into *SacI/XhoI* sites of pET22b (+), resulting in pET22b-Cys₃-EC1-5-His₆. The insertion of the plasmid was confirmed by sequencing. The pET22b-Cys₃-EC1-5-His₆ was transformed into BL21 (DE3) pLysS cells. The transformed cells were inoculated into 400 ml LB medium (containing Amp) and incubated at 37 °C until OD₆₀₀ reached to 0.6 (about 3 h). The following induction of the cells was carried out with 1 mM IPTG at 18 °C for 16 h. The cell pellet was then centrifuged at 8000 rpm and resuspended in 20 ml of binding buffer (50 mM sodium phosphate buffer pH 7.4, 150 mM NaCl, and 10 mM imidazole). The resuspended cells were sonicated for 5 min on ice and centrifuged for 10 min at 4 °C. The supernatant was utilized for protein purification with TALON Metal Affinity Resin (Clontech, Mountain View, CA) following the manufacturer's instructions.

AFM experiment

The AFM experiments were implemented in a HEPES buffer with pH 7.4 and 1 mM Ca²⁺ using a DI multi-mode AFM with picoforce system (Veeco instrument, NY). The glass slides (Deckglaser, German) were treated in a chemical vapor deposition system (Denton discovery, NJ), and 5 nm chromium and 20 nm gold were deposited. E-cadherin Cys₃-EC1-5-His₆ solution (0.5 μg/mL) was incubated on the gold-covered slides for 15 min before the AFM experiments. In each pulling cycle, the silicon tip of the cantilever (Appnano, HYDRA2R-100NG) was pushed against the slide for 2 s at a force of 800 pN. Then, the tip was withdrawn for 600 nm. Once a protein molecule was picked up and stretched, a force-extension curve with saw-tooth patterns (Figure 2 (a) inset) could be recorded. The constant velocity of 600 nm/s was used. The spring constant of the cantilever was between 12 and 20 pN/nm. The force extension trajectories were fitted by WLC model, $FP/k_B T = (1/4)(1 - (x/L))^{-2} - (1/4) + (x/L)$ (Fisher, Oberhauser, Carrion-Vazquez, Marszalek, & Fernandez, 1999; Rief et al., 1997), where F is the external force, P is the persistence length determined by the molecule stiffness, k_B is the Boltzmann constant, T is the temperature (295 K), L is the contour length of molecule, and x is the extension of molecule. Here, the persistence length was kept at 0.4 nm and the contour length varied with each force peak, e.g. L_1 and L_2 in the inset of Figure 2(a). The peak force, where unfolding happened, was recorded as the unfolding force, F , and the increase in contour length was recorded as contour length change, ΔL .

In the analysis of the experimental data from AFM measurements, we chose all trajectories showing three or more force peaks. Typically, the first force peak at a small extension (< 5 nm) in the trajectories probably corresponded to the interaction between the tip and the substrate. These force peaks could also not be fitted well with WLC model, while other force peaks could. This suggested that the rest of the force peaks were from stretching the polymer chains of the proteins. For each ΔL , two sequential good force peaks were needed, so trajectories with at least three force peaks were chosen for analysis.

Abbreviations

AFM	atomic force microscopy
CAD8	cadherin 8
CAD8-D	dimer of cadherin 8
CAD11	cadherin 11
CAD11-D	dimer of cadherin 11
CCAD	C-cadherin
CCAD-D	dimer of C-cadherin
EC	extracellular cadherin
EC1	the first extracellular cadherin
EC2	the second extracellular cadherin
EC1–2	the first two extracellular cadherin
ECAD	E-cadherin
ECAD-D	dimer of E-cadherin
ECAD-NOCA	E-cadherin without Ca ²⁺
NCAD-D	dimer of N-cadherin
PCR	polymerase chain reaction
SMD	steered molecular dynamics
VMD	visual molecular dynamics
WLC	worm-like-chain

Acknowledgements

We would like thank the Computer Center under the office of Deputy President and Center for Computational Science and Engineering at National University of Singapore for providing the computational service for simulations done in this paper. We gratefully acknowledge support from MechanoBiology Institute Seed grant (WBS R-714-002-007-271).

Supplementary material

The supplementary material for this paper is available online at <http://dx.doi.10.1080/07391102.2012.726530>.

References

- Baumgartner, W., Hinterdorfer, P., Ness, W., Raab, A., Vestweber, D., Schindler, H., & Drenckhahn, D. (2000). Cadherin interaction probed by atomic force microscopy. *Proceedings of the National Academy of Sciences of the United States of America*, *97*, 4005–4010.
- Bayas, M. V., Leung, A., Evans, E., & Leckband, D. (2006). Lifetime measurements reveal kinetic differences between homophilic cadherin bonds. *Biophysical Journal*, *90*, 1385–1395.

- Bayas, M. V., Schulten, K., & Leckband, D. (2004). Forced dissociation of the strand dimer interface between C-cadherin ectodomains. *Mechanics and Chemistry of Biosystems, 1*, 101–111.
- Boggon, T. J., Murray, J., Chappuis-Flament, S., Wong, E., Gumbiner, B. M., & Shapiro, L. (2002). C-cadherin ectodomain structure and implications for cell adhesion mechanisms. *Science, 296*, 1308–1313.
- Cailliez, F., & Lavery, R. (2005). Cadherin mechanics and complexation: The importance of calcium binding. *Biophysical Journal, 89*, 3895–3903.
- Chu, Y. S., Eder, O., Thomas, W. A., Simcha, I., Pincet, F., Ben-Ze'ev, A., ... Dufour, S. (2006). Prototypical type I E-cadherin and type II cadherin-7 mediate very distinct adhesiveness through their extracellular domains. *Journal of Biological Chemistry, 281*, 2901–2910.
- Chu, Y. S., Thomas, W. A., Eder, O., Pincet, F., Perez, E., Thiery, J. P., & Dufour, S. (2004). Force measurements in E-cadherin-mediated cell doublets reveal rapid adhesion strengthened by actin cytoskeleton remodeling through Rac and Cdc42. *Journal of Cell Biology, 167*, 1183–1194.
- Cowin, P., Rowlands, T. M., & Hatsell, S. J. (2005). Cadherins and catenins in breast cancer. *Current Opinion in Cell Biology, 17*, 499–508.
- del Rio, A., Perez-Jimenez, R., Liu, R., Roca-Cusachs, P., Fernandez, J. M., & Sheetz, M. P. (2009). Stretching single talin rod molecules activates vinculin binding. *Science, 323*, 638–641.
- Evans, E. A., & Calderwood, D. A. (2007). Forces and bond dynamics in cell adhesion. *Science, 316*, 1148–1153.
- Fisher, T. E., Oberhauser, A. F., Carrion-Vazquez, M., Marszalek, P. E., & Fernandez, J. M. (1999). The study of protein mechanics with the atomic force microscope. *Trends in Biochemical Sciences, 24*, 379–384.
- Gao, M., Sotomayor, M., Villa, E., Lee, E. H., & Schulten, K. (2006). Molecular mechanisms of cellular mechanics. *Physical Chemistry Chemical Physics, 8*, 3692–3706.
- Garcia-Manyes, S., Brujic, J., Badilla, C. L., & Fernandez, J. M. (2007). Force-clamp spectroscopy of single-protein monomers reveals the individual unfolding and folding pathways of I27 and ubiquitin. *Biophysical Journal, 93*, 2436–2446.
- Gumbiner, B. M. (1996). Cell adhesion: The molecular basis of tissue architecture and morphogenesis. *Cell, 84*, 345–357.
- Gumbiner, B. M. (2005). Regulation of cadherin-mediated adhesion in morphogenesis. *Nature Reviews Molecular Cell Biology, 6*, 622–634.
- Harrison, O. J., Jin, X., Hong, S., Bahna, F., Ahlsen, G., Brasch, J., ... Honig, B. (2011). The extracellular architecture of adherens junctions revealed by crystal structures of type I cadherins. *Structure, 19*, 244–256.
- Hatta, K., Nose, A., Nagafuchi, A., & Takeichi, M. (1988). Cloning and expression of cDNA encoding a neural calcium-dependent cell adhesion molecule: Its identity in the cadherin gene family. *Journal of Cell Biology, 106*, 873–881.
- Humphrey, W., Dalke, A., & Schulten, K. (1996). VMD: Visual molecular dynamics. *Journal of Molecular Graphics, 14*(33–38), 27–38.
- Jorgensen, W. L., Chandrasekhar, J., Madura, J. D., Impey, R. W., & Klein, M. L. (1983). Comparison of simple potential functions for simulating liquid water. *Journal of Chemical Physics, 79*, 926–935.
- Koch, A. W., Pokutta, S., Lustig, A., & Engel, J. (1997). Calcium binding and homoassociation of E-cadherin domains. *Biochemistry, 36*, 7697–7705.
- Mackerell, A. D. Jr., Feig, M., & Brooks, C. L. III (2004). Extending the treatment of backbone energetics in protein force fields: Limitations of gas-phase quantum mechanics in reproducing protein conformational distributions in molecular dynamics simulations. *Journal of Computational Chemistry, 25*, 1400–1415.
- May, C., Doody, J. F., Abdullah, R., Balderes, P., Xu, X., Chen, C. P., ... Bohlen, P. (2005). Identification of a transiently exposed VE-cadherin epitope that allows for specific targeting of an antibody to the tumor neovasculature. *Blood, 105*, 4337–4344.
- Nollet, F., Kools, P., & van Roy, F. (2000). Phylogenetic analysis of the cadherin superfamily allows identification of six major subfamilies besides several solitary members. *Journal of Molecular Biology, 299*, 551–572.
- Oroz, J., Valbuena, A., Vera, A. M., Mendieta, J., Gomez-Puertas, P., & Carrion-Vazquez, M. (2011). Nanomechanics of the Cadherin Ectodomain 'Canalization' BYCa2 binding results in a new mechanical element. *Journal of Biological Chemistry, 286*, 9405–9418.
- Overduin, M., Harvey, T. S., Bagby, S., Tong, K. I., Yau, P., Takeichi, M., & Ikura, M. (1995). Solution structure of the epithelial cadherin domain responsible for selective cell adhesion. *Science, 267*, 386–389.
- Panorchan, P., George, J. P., & Wirtz, D. (2006a). Probing intercellular interactions between vascular endothelial cadherin pairs at single-molecule resolution and in living cells. *Journal of Molecular Biology, 358*, 665–674.
- Panorchan, P., Thompson, M. S., Davis, K. J., Tseng, Y., Konstantopoulos, K., & Wirtz, D. (2006b). Single-molecule analysis of cadherin-mediated cell–cell adhesion. *Journal of Cell Science, 119*, 66–74.
- Patel, S. D., Ciatto, C., Chen, C. P., Bahna, F., Rajebhosale, M., Arkus, N., ... Shapiro, L. (2006). Type II cadherin ectodomain structures: Implications for classical cadherin specificity. *Cell, 124*, 1255–1268.
- Perret, E., Leung, A., Feracci, H., & Evans, E. (2004). Trans-bonded pairs of E-cadherin exhibit a remarkable hierarchy of mechanical strengths. *Proceedings of the National Academy of Sciences of the United States of America, 101*, 16472–16477.
- Phillips, J. C., Braun, R., Wang, W., Gumbart, J., Tajkhorshid, E., Villa, E., ... Schulten, K. (2005). Scalable molecular dynamics with NAMD. *Journal of Computational Chemistry, 26*, 1781–1802.
- Pla, P., Moore, R., Morali, O. G., Grille, S., Martinuzzi, S., Delmas, V., & Larue, L. (2001). Cadherins in neural crest cell development and transformation. *Journal of Cellular Physiology, 189*, 121–132.
- Rief, M., Gautel, M., Oesterhelt, F., Fernandez, J. M., & Gaub, H. E. (1997). Reversible unfolding of individual titin immunoglobulin domains by AFM. *Science, 276*, 1109–1112.
- Shan, W. S., Koch, A., Murray, J., Colman, D. R., & Shapiro, L. (1999). The adhesive binding site of cadherins revisited. *Biophysical Chemistry, 82*, 157–163.
- Shapiro, L., Fannon, A. M., Kwong, P. D., Thompson, A., Lehmann, M. S., Grubel, G., ... Hendrickson, W. A. (1995). Structural basis of cell-cell adhesion by cadherins. *Nature, 374*, 327–337.
- Shi, Q. M., Maruthamuthu, V., Li, F., & Leckband, D. (2010). Allosteric cross talk between cadherin extracellular domains. *Biophysical Journal, 99*, 95–104.
- Sivasankar, S., Briehar, W., Lavrik, N., Gumbiner, B., & Leckband, D. (1999). Direct molecular force measurements of multiple adhesive interactions between cadherin

- ectodomains. *Proceedings of the National Academy of Sciences of the United States of America*, *96*, 11820–11824.
- Sivasankar, S., Gumbiner, B., & Leckband, D. (2001). Direct measurements of multiple adhesive alignments and unbinding trajectories between cadherin extracellular domains. *Biophysical Journal*, *80*, 1758–1768.
- Sivasankar, S., Zhang, Y., Nelson, W. J., & Chu, S. (2009). Characterizing the initial encounter complex in cadherin adhesion. *Structure*, *17*, 1075–1081.
- Sotomayor, M., Corey, D. P., & Schulten, K. (2005). In search of the hair-cell gating spring: Elastic properties of ankyrin and cadherin repeats. *Structure*, *13*, 669–682.
- Sotomayor, M., & Schulten, K. (2008). The allosteric role of the Ca^{2+} switch in adhesion and elasticity of C-cadherin. *Biophysical Journal*, *94*, 4621–4633.
- Sotomayor, M., Weihofen, W. A., Gaudet, R., & Corey, D. P. (2010). Structural determinants of cadherin-23 function in hearing and deafness. *Neuron*, *66*, 85–100.
- Takeichi, M. (1995). Morphogenetic roles of classic cadherins. *Current Opinion in Cell Biology*, *7*, 619–627.
- Tamura, K., Shan, W. S., Hendrickson, W. A., Colman, D. R., & Shapiro, L. (1998). Structure–function analysis of cell adhesion by neural (N-) cadherin. *Neuron*, *20*, 1153–1163.
- Thiery, J. P., Engl, W., Viasnoff, V., & Dufour, S. (in press). Biochemical and biophysical origins of cadherin selectivity and adhesion strength. *Current Opinion in Cell Biology*.
- van Roy, F., & Berx, G. (2008). The cell-cell adhesion molecule E-cadherin. *Cellular and Molecular Life Sciences*, *65*, 3756–3788.
- Wu, F., Lu, C., Thiery, J. P., Lim, C. T., Shen, S., Zhong, S., & Liu, R. (2012). Dynamics of E-cadherin extracellular domains: Partial unfolding and intermediate states. *Manuscript submitted for publication*.
- Wu, Y., Vendome, J., Shapiro, L., Ben-Shaul, A., & Honig, B. (2011). Transforming binding affinities from three dimensions to two with application to cadherin clustering. *Nature*, *475*, 510–513.
- Zhang, Y. X., Sivasankar, S., Nelson, W. J., & Chu, S. (2009). Resolving cadherin interactions and binding cooperativity at the single-molecule level. *Proceedings of the National Academy of Sciences of the United States of America*, *106*, 109–114.
- Zhu, B., Chappuis-Flament, S., Wong, E., Jensen, I. E., Gumbiner, B. M., & Leckband, D. (2003). Functional analysis of the structural basis of homophilic cadherin adhesion. *Biophysical Journal*, *84*, 4033–4042.